SCIENCE CHINA
Technological Sciences

• Article •

February 2014 Vol.57 No.2: 368–378
doi: 10.1007/s11431-013-5416-x

A reduced-order-model-based multiple-in multiple-out gust alleviation control law design method in transonic flow

CHEN Gang*, WANG Xian & LI YueMing

State Key Laboratory for Strength and Vibration of Mechanical Structures, School of Aerospace, Xi'an Jiaotong University, Xi'an 710049, China

Received June 15, 2013; accepted October 12, 2013; published online December 13, 2013

Gust alleviation is very important to a large flexible aircraft. A nonlinear low-order aerodynamic state space model is required to model the nonlinear aeroelastic responses due to gust. Based on the proper orthogonal decomposition method, a reduced order modeling of gust loads was proposed. And then the open-loop and closed-loop reduced order state space model for the transonic aeroelastic system was developed. The static output feed back control scheme was used to design a simple multiple-in multiple-out (MIMO) gust alleviation control law. The control law was demonstrated with the Goland+ wing model with four control surfaces. The simulation results of different discrete gusts show the capability and good performance of the designed MIMO controller in transonic gust alleviation.

transonic gust alleviation, reduced order model, proper orthogonal decomposition, static output feed back

Citation: Chen G, Wang X, Li Y M. A reduced-order-model-based multiple-in multiple-out gust alleviation control law design method in transonic flow. Sci China Tech Sci, 2014, 57: 368–378, doi: 10.1007/s11431-013-5416-x

1 Introduction

Gust loads can reduce the ride quality and structural fatigue life of aircrafts. Over the past decades, gust analyses have become one of the standard parts of aircraft design. The tendency to reduce weight and operating speed by using light-weight composite materials greatly increases structural flexibility of modern aircrafts. The flexible aircraft structure must withstand discrete gusts of certain profile, intensity and gradient [1]. In recent years, gust load alleviation has become one of the focuses in active control technology for modern large flexible aircrafts. The active gust alleviation system aims to control gust effects on flexible aircraft structures and improve aircraft stability and ride quality, such as the Active Aeroelastic Wing (AAW) program [2], the European Active Aeroelastic Aircraft Structures (3AS) wing program [3], and the Truss Braced Wing (TBW) configuration [4].

Many control methods have been applied to design gust alleviation control laws for aerodynamic control surfaces [2–9]. Most of these investigations and traditional industrial applications concentrate on low-speed or subsonic fight regime. The unsteady aerodynamic responses are nearly entirely linear and therefore the gust load models typically rely on linear aerodynamic methods [10]. However, in the transonic regime, the unsteady aerodynamic forces are no longer linearly dependent on the flow parameters, i.e., the angle of attack and Mach number. Thus gust loads cannot be accurately predicted by linear aerodynamic models [11, 12]. On the other hand, with the increase of the structural flexibility, fast accurate calculation of elastic generalized aerodynamic forces (GAFs) has been a major challenge in aeroservoelastic analysis and optimization. The design experiences in new flexible aircraft configuration such as high

*Corresponding author (email: aachengang@mail.xjtu.edu.cn)

altitude long endurance (HALE) and the Helios crash investigation also indicate that gust response analysis has to be supported with some nonlinear aerodynamic models and nonlinear aeroservoelastic codes [13, 14].

As a benefit of the development of computational aeroelasticity, reduced-order modeling (ROM) of nonlinear unsteady aerodynamics has been popular in transonic aeroelastic analysis. ROM seeks to capture the dominant nonlinear behaviors of aeroelastic systems with a simple mathematical representative model constructed from the full-order system. Different approaches for constructing ROMs have been proposed, i.e., the system identification-based models [15, 16], the flow eigenmode-based models [17, 18], and the nonlinear dynamic theory based models [19, 20]. ROMs have been widely used to make nonlinear aeroelastic response prediction (i.e. flutter and limit cycle oscillation) in transonic flow regime [15–20] and active flutter control law design [21–26].

Although great achievements have been made in nonlinear aeroelastic stability analysis, ROMs are still scarcely applied to gust responses analysis and alleviation. Recently, Raveh presented ROM of the nonlinear aerodynamic gust forces in transonic flow for a clamped rigid wing and an elastic aircraft, including two parametric auto-regressive and moving average models (ARMA) and state-space models [11, 12, 25]. Volterra-based ROM has also been used to design gust load alleviation controller for a highly flexible aircraft [16]. Ronch and Badcock successfully extended their third-order nonlinear ROM to gust load alleviation control design for a pitch-plunge aerofoil with structural nonlinearities [17]. However, as one of the most popular and promising ROMs, proper orthogonal decomposition (POD) method is still seldom applied in gust loads alleviation. Rather than only being capable of predicting integrated coefficient time histories (i.e. ARMA/ROM and Volterra/ROM), POD/ROM can provide the time history responses of the distributed surface pressures to arbitrary inputs [17, 18, 20], as well as suitable for an arbitrary gust input [14].

The contribution of this paper is to develop a gust alleviation control law design method based on POD/ROM that is suitable for a flexible aircraft in transonic flow regime. The usage of multiple control surfaces can simultaneously reduce aerodynamic drags and gust loads, increase flight safety and comfort, and improve the aeroelastic control performance of flexible aircrafts [2–4, 27–30]. Thus the proposed gust alleviation control law design method is demonstrated by a flexible wing with four control surfaces. The designed multiple-in multiple-out (MIMO) control law is expected to reduce the gust loads to the structure (for structural fatigue life) and unsteady aerodynamic coefficients (for ride quality) simultaneously.

2 ROM of gust alleviation system

2.1 The full-order discretized aeroelastic equation under gust

For a fully coupled nonlinear aeroelastic system, the Euler/Navier-Stokes equation discretized by the finite volume method is written as follows:

$$\frac{\mathrm{d}\left(\boldsymbol{A}(\boldsymbol{u})\boldsymbol{w}\right)}{\mathrm{d}t}+\boldsymbol{F}\left(\boldsymbol{w},\boldsymbol{u},\dot{\boldsymbol{u}},\boldsymbol{w}_{\mathrm{g}}\right)=0, \tag{1}$$

where $\boldsymbol{w}$ is the conservative fluid state variable, $\boldsymbol{F}$ is the nonlinear flux function, $\boldsymbol{A}$ is the fluid cell volume matrix, u is the position vector of the fluid grid points, and $\boldsymbol{w}_{\mathrm{g}}$ is the gust velocity. Supposing that $\Delta\boldsymbol{w},\Delta\boldsymbol{u},\Delta\dot{\boldsymbol{u}}$ are the small perturbations around the nonlinear steady state variables $\left(\boldsymbol{w}_0,\boldsymbol{u}_0,\dot{\boldsymbol{u}}_0\right)$, the full-order dynamical linearization of the unsteady fluid equation around the nonlinear steady flow can be derived by the Taylor expansion [17, 23]:

$$\begin{cases}\boldsymbol{A}_0\Delta\dot{\boldsymbol{w}}+\boldsymbol{H}_0\Delta\boldsymbol{w}+\boldsymbol{G}_0\Delta\boldsymbol{u}+\left(\boldsymbol{C}_0+\boldsymbol{E}_0\right)\Delta\dot{\boldsymbol{u}}+\boldsymbol{D}_0\Delta\boldsymbol{w}_{\mathrm{g}}=0,\\ \boldsymbol{H}_0=\dfrac{\partial\boldsymbol{F}}{\partial\boldsymbol{w}}\left(\boldsymbol{w}_0,\boldsymbol{u}_0,\dot{\boldsymbol{u}}_0,\boldsymbol{w}_{\mathrm{g}0}\right),\\ \boldsymbol{E}_0=\boldsymbol{w}_0\dfrac{\partial\boldsymbol{A}}{\partial\dot{\boldsymbol{u}}}\left(\boldsymbol{u}_0\right),\boldsymbol{C}_0=\dfrac{\partial\boldsymbol{F}}{\partial\dot{\boldsymbol{u}}}\left(\boldsymbol{w}_0,\boldsymbol{u}_0,\dot{\boldsymbol{u}}_0,\boldsymbol{w}_{\mathrm{g}0}\right),\\ \boldsymbol{D}_0=\dfrac{\partial\boldsymbol{F}}{\partial\boldsymbol{w}_{\mathrm{g}}}\left(\boldsymbol{w}_0,\boldsymbol{u}_0,\dot{\boldsymbol{u}}_0,\boldsymbol{w}_{\mathrm{g}0}\right),\boldsymbol{G}_0=\dfrac{\partial\boldsymbol{F}}{\partial\boldsymbol{u}}\left(\boldsymbol{w}_0,\boldsymbol{u}_0,\dot{\boldsymbol{u}}_0,\boldsymbol{w}_{\mathrm{g}0}\right),\end{cases} \tag{2}$$

where $\boldsymbol{A}_0$ is the volume of the fluid cell in the steady state. To simplify the notation, $\boldsymbol{w},\boldsymbol{u},\dot{\boldsymbol{u}}$ are used to represent the perturbation variables $\Delta\boldsymbol{w},\Delta\boldsymbol{u},\Delta\dot{\boldsymbol{u}}$, respectively.

The structural dynamic equation discretized by the finite element method is written as follows [31, 32]:

$$\boldsymbol{M}\boldsymbol{v}_{\mathrm{t}}+\boldsymbol{C}_{\mathrm{s}}\boldsymbol{v}_{\mathrm{s}}+\boldsymbol{K}\boldsymbol{u}_{\mathrm{s}}=\boldsymbol{q}_{\infty}\boldsymbol{f}^{\mathrm{ext}}\left(\boldsymbol{u}_{\mathrm{s}},\boldsymbol{w},\boldsymbol{w}_{\mathrm{g}}\right), \tag{3}$$

where $\boldsymbol{u}_{\mathrm{s}},\boldsymbol{v}_{\mathrm{s}}$ are the displacement and velocity vectors of the structural grids, and $\boldsymbol{M},\boldsymbol{C}_{\mathrm{s}}$ are the structural element mass matrix and structural damping matrix. In the unsteady transonic flow with gust, the nonlinear unsteady external forces $\boldsymbol{f}^{\mathrm{ext}}$ acting at the structural grid points are represented as

$$\begin{aligned}\boldsymbol{f}^{\mathrm{ext}}\left(\boldsymbol{u}_{\mathrm{s}},\boldsymbol{w},\boldsymbol{w}_{\mathrm{g}}\right)=&\,\boldsymbol{q}_{\infty}\frac{\partial\boldsymbol{f}^{\mathrm{ext}}}{\partial\boldsymbol{u}_{\mathrm{s}}}\left(\boldsymbol{u}_{\mathrm{s}0},\boldsymbol{w}_0,\boldsymbol{w}_{\mathrm{g}}\right)\boldsymbol{u}_{\mathrm{s}}\\&+\boldsymbol{q}_{\infty}\frac{\partial\boldsymbol{f}^{\mathrm{ext}}}{\partial\boldsymbol{w}}\left(\boldsymbol{u}_{\mathrm{s}0},\boldsymbol{w}_0,\boldsymbol{w}_{\mathrm{g}}\right)\boldsymbol{w}\\&+\boldsymbol{q}_{\infty}\frac{\partial\boldsymbol{f}^{\mathrm{ext}}}{\partial\boldsymbol{w}_{\mathrm{g}}}\left(\boldsymbol{u}_{\mathrm{s}0},\boldsymbol{w}_0,\boldsymbol{w}_{\mathrm{g}}\right)\boldsymbol{w}_{\mathrm{g}},\end{aligned} \tag{4}$$

where the first, second and third right items are the unsteady

aerodynamic influence forces related to the structural deformation, the flow flux variables and the gust velocity, respectively. Letting

$$\boldsymbol{P}_{\mathrm{w}}=\frac{\partial \boldsymbol{f}^{\mathrm{ext}}}{\partial \boldsymbol{w}}\left(\boldsymbol{u}_{\mathrm{s}0},\boldsymbol{w}_0,\boldsymbol{w}_{\mathrm{g}0}\right),\ \boldsymbol{P}_{\mathrm{w_g}}=\frac{\partial \boldsymbol{f}^{\mathrm{ext}}}{\partial \boldsymbol{w}_{\mathrm{g}}}\left(\boldsymbol{u}_{\mathrm{s}0},\boldsymbol{w}_0,\boldsymbol{w}_{\mathrm{g}0}\right),$$
$$\boldsymbol{K}_{\mathrm{f}}=\frac{\partial \boldsymbol{f}^{\mathrm{ext}}}{\partial \boldsymbol{u}_{\mathrm{s}}}\left(\boldsymbol{u}_{\mathrm{s}0},\boldsymbol{w}_0,\boldsymbol{w}_{\mathrm{g}0}\right), \tag{5}$$

the full-order discretized unsteady flow eq. (2), named snapshot equation, can be transformed into a state space equation:

$$\begin{cases}\dot{\boldsymbol{w}}=\tilde{\boldsymbol{A}}\boldsymbol{w}+\tilde{\boldsymbol{B}}\left[\boldsymbol{v}\quad \boldsymbol{u}_{\mathrm{s}}\right]^{\mathrm{T}}+\tilde{\boldsymbol{D}}\boldsymbol{w}_{\mathrm{g}},\\ \boldsymbol{y}_1=\tilde{\boldsymbol{C}}\boldsymbol{w}+\tilde{\boldsymbol{D}}_{\mathrm{g}}\boldsymbol{w}_{\mathrm{g}},\end{cases} \tag{6}$$

where

$$\tilde{\boldsymbol{A}}=-\boldsymbol{A}_0^{-1}\boldsymbol{H}_0,\ \tilde{\boldsymbol{B}}=-\boldsymbol{A}_0^{-1}\left(\boldsymbol{E}_0+\boldsymbol{C}_0\quad \boldsymbol{G}_0\right),$$
$$\tilde{\boldsymbol{D}}=-\boldsymbol{A}_0^{-1}\boldsymbol{D}_0,\quad \tilde{\boldsymbol{C}}=\tfrac{1}{2}\rho_\infty V^2\boldsymbol{P}_{\mathrm{w}}=q_\infty\boldsymbol{P}_{\mathrm{w}},\ \tilde{\boldsymbol{D}}_{\mathrm{g}}=q_\infty\boldsymbol{P}_{\mathrm{w_g}}.$$

The output y_1 denotes the external aerodynamic forces acting on wing structure including the unsteady aerodynamic loads due to the gust and the flow flux.

Combining the structural eq. (3) with the fluid eq. (6), the fully coupled full-order dynamical linearization of the aeroelastic state-space model is obtained:

$$\begin{bmatrix}\dot{\boldsymbol{w}}\\ \dot{\boldsymbol{v}}\\ \dot{\boldsymbol{u}}_{\mathrm{s}}\end{bmatrix}=\begin{bmatrix}-\boldsymbol{A}_0^{-1}\boldsymbol{H}_0 & -\boldsymbol{A}_0^{-1}\left(\boldsymbol{E}_0+\boldsymbol{C}_0\right) & -\boldsymbol{A}_0^{-1}\boldsymbol{G}_0\\ q_\infty\boldsymbol{M}^{-1}\boldsymbol{P}_{\mathrm{w}} & -\boldsymbol{M}^{-1}\boldsymbol{C}_{\mathrm{s}} & -\boldsymbol{M}^{-1}\boldsymbol{K}_{\mathrm{s}}\\ 0 & I & 0\end{bmatrix}\begin{bmatrix}\boldsymbol{w}\\ \boldsymbol{v}\\ \boldsymbol{u}_{\mathrm{s}}\end{bmatrix}+\begin{bmatrix}\tilde{\boldsymbol{D}}\\ q_\infty\boldsymbol{M}^{-1}\boldsymbol{P}_{\mathrm{w_g}}\\ 0\end{bmatrix}\boldsymbol{w}_{\mathrm{g}}, \tag{7}$$

where $\boldsymbol{K}_{\mathrm{s}}=\boldsymbol{K}-\boldsymbol{K}_{\mathrm{f}}$. With a large mount of flow meshes, the direct time-marching computation of the above full-order aeroelastic equation is too expensive for the near real time simulation. It is also impractical and not capable of designing active gust alleviation and flutter controllers because of the large order of the full-order equation. Therefore, the full-order discretized aeroelastic system of eq. (7) should be reduced to a much lower order model that can predict the unsteady gust loads in near real time. Here snapshots-based POD model reduction method is used to realize such objective [17, 23].

2.2 Snapshot-POD based reduced order model

For one series of system snapshot data $\left\{\boldsymbol{x}^k\right\}$, $\boldsymbol{x}^k\in\boldsymbol{C}^n$ in the n-dimensional space, the POD method seeks to find an m-dimensional proper orthogonal subspace $\boldsymbol{\Psi}\in\boldsymbol{R}^{n\times m}$ to minimize the mapping errors from $\left\{\boldsymbol{x}^k\right\}$ to $\boldsymbol{\Psi}$. The constraint optimization problem is equivalent to [17, 33, 34]

$$\boldsymbol{H}=\max_{\boldsymbol{\Phi}}\sum_{k=1}^{m}\frac{\left\langle\left(\boldsymbol{x}^k,\boldsymbol{\Phi}\right)^2\right\rangle}{\left\|\boldsymbol{\Phi}\right\|^2}=\sum_{k=1}^{m}\frac{\left\langle\left(\boldsymbol{x}^k,\boldsymbol{\Psi}\right)^2\right\rangle}{\left\|\boldsymbol{\Psi}\right\|^2},\boldsymbol{\Phi}^{\mathrm{H}}\boldsymbol{\Phi}=\boldsymbol{I} \tag{8}$$

and then it is transformed into a Lagrange equation:

$$J\left(\boldsymbol{\Phi}\right)=\sum_{k=1}^{m}\left(\boldsymbol{x}^k,\boldsymbol{\Phi}\right)^2-\boldsymbol{\lambda}\left(\left\|\boldsymbol{\Phi}\right\|-1\right). \tag{9}$$

By solving the partial derivative objective function $J\left(\boldsymbol{\Phi}\right)$ with respect to $\boldsymbol{\Phi}$, there is

$$\frac{\mathrm{d}}{\mathrm{d}\boldsymbol{\Phi}}\boldsymbol{J}\left(\boldsymbol{\Phi}\right)=2\boldsymbol{X}\boldsymbol{X}^{\mathrm{H}}\boldsymbol{\Phi}-2\lambda\boldsymbol{\Phi}, \tag{10}$$

where $\boldsymbol{X}=\left\{x^1,\cdots,x^m\right\}$ is the matrix of snapshots which is the time responses of unsteady aerodynamic forces related to gust and structural movements. The snapshots can be calculated from the full-order dynamical linearization of the discretized aeroelastic snapshot eq. (6) by inputting some special training signals such as Dirac function signals to structural grids or a Gaussian doublet (zero mean) gust velocity profile [10, 23]. Eq. (10) is then set equal to zero, thus,

$$\left(\boldsymbol{X}\boldsymbol{X}^{\mathrm{H}}-\lambda\boldsymbol{I}\right)\boldsymbol{\Psi}=0. \tag{11}$$

Because $\boldsymbol{X}\boldsymbol{X}^{\mathrm{H}}$ and $\boldsymbol{X}^{\mathrm{H}}\boldsymbol{X}$ have the same eigenvalues, $\boldsymbol{\Psi}$ can be calculated from the following m-dimensional equivalent equation:

$$\begin{cases}\boldsymbol{X}^{\mathrm{H}}\boldsymbol{X}\boldsymbol{V}=\boldsymbol{V}\boldsymbol{\Lambda},\\ \boldsymbol{\Psi}=\boldsymbol{X}\boldsymbol{V}\boldsymbol{\Lambda}^{-1/2},\end{cases} \tag{12}$$

where $\boldsymbol{\Psi}=\left[\psi_1\quad\psi_2\quad\cdots\quad\psi_l\right]$, $\boldsymbol{\Lambda}=\mathrm{diag}\left(\lambda_1\quad\lambda_2\quad\cdots\quad\lambda_l\right)$, and $\lambda_1\geqslant\lambda_2\geqslant\cdots\geqslant\lambda_l$. By retaining the leading r-order vectors and constructing a new eigenmode matrix $\boldsymbol{\Psi}_r=\left[\psi_1\quad\psi_2\quad\cdots\quad\psi_r\right]$, the full-order series $x^{n\times1}$ can be reduced to a lower r-order system:

$$\boldsymbol{x}^{n\times1}=\boldsymbol{\Psi}_r\boldsymbol{\xi}^{r\times1}. \tag{13}$$

Introducing the following relationship equations:

$$\boldsymbol{w}^{n\times1}=\boldsymbol{\Psi}_{\mathrm{r}}w_{\mathrm{r}}^{r\times1},\ \boldsymbol{u}_{\mathrm{s}}=\boldsymbol{\Psi}_{\mathrm{m}}u_{\mathrm{m}},\ \boldsymbol{M}_{\mathrm{m}}=\boldsymbol{\Psi}_{\mathrm{m}}^{\mathrm{T}}M\boldsymbol{\Psi}_{\mathrm{m}},$$
$$\boldsymbol{C}_{\mathrm{m}}=\boldsymbol{\Psi}_{\mathrm{m}}^{\mathrm{T}}\boldsymbol{C}_{\mathrm{s}}\boldsymbol{\Psi}_{\mathrm{m}},\ K_{\mathrm{m}}=\boldsymbol{\Psi}_{\mathrm{m}}^{\mathrm{T}}\boldsymbol{K}_{\mathrm{s}}\boldsymbol{\Psi}_{\mathrm{m}}, \tag{14}$$

where $\boldsymbol{\Psi}_{\mathrm{r}}$ denote the eigenmodes of the snapshot matrix and $\boldsymbol{\Psi}_{\mathrm{m}}$ denotes the structural modal, the r-order POD/ROM of the aeroelastic system in the generalized coordinates is obtained as [25, 33]

$$\begin{bmatrix} \dot{\boldsymbol{w}}_{\mathrm{r}} \\ \dot{\boldsymbol{v}}_{\mathrm{m}} \\ \dot{\boldsymbol{u}}_{\mathrm{m}} \end{bmatrix} = \begin{bmatrix} -\boldsymbol{\Psi}_{\mathrm{r}}^{\mathrm{T}}\boldsymbol{A}_0^{-1}\boldsymbol{H}\boldsymbol{\Psi}_{\mathrm{r}} & -\boldsymbol{\Psi}_{\mathrm{r}}^{\mathrm{T}}\boldsymbol{A}_0^{-1}\left(\boldsymbol{E}+\boldsymbol{C}\right)\boldsymbol{\Psi}_{\mathrm{m}} & -\boldsymbol{\Psi}_{\mathrm{r}}^{\mathrm{T}}\boldsymbol{A}_0^{-1}\boldsymbol{G}\boldsymbol{\Psi}_{\mathrm{m}} \\ q_\infty \boldsymbol{M}_{\mathrm{m}}^{-1}\boldsymbol{\Psi}_{\mathrm{m}}^{\mathrm{T}}\boldsymbol{P}_{\mathrm{w}}\boldsymbol{\Psi}_{\mathrm{r}} & -\boldsymbol{M}_{\mathrm{m}}^{-1}\boldsymbol{C}_{\mathrm{m}} & -\boldsymbol{M}_{\mathrm{m}}^{-1}\boldsymbol{K}_{\mathrm{m}} \\ \boldsymbol{0} & \boldsymbol{I} & \boldsymbol{0} \end{bmatrix} \times \begin{bmatrix} \boldsymbol{w}_{\mathrm{r}} \\ \boldsymbol{v}_{\mathrm{m}} \\ \boldsymbol{u}_{\mathrm{m}} \end{bmatrix} + \begin{bmatrix} -\boldsymbol{\Psi}_{\mathrm{r}}^{\mathrm{T}}\tilde{\boldsymbol{D}} \\ q_\infty \boldsymbol{\Psi}_{\mathrm{m}}^{\mathrm{T}}\boldsymbol{M}^{-1}\boldsymbol{P}_{\boldsymbol{w}_{\mathrm{g}}} \\ 0 \end{bmatrix} \boldsymbol{w}_{\mathrm{g}}. \tag{15}$$

The order of the gust POD/ROM in eq. (15) is much smaller than that of the original full-order system (7). It is very convenient for the fast analysis of the system performance and is more efficient than the full-order unsteady CFD/CSD computation. If a gust velocity profile $\boldsymbol{w}_{\mathrm{g}}$ is given, the gust responses of the aeroelastic system can be calculated in near real time. For the convenience of controller design, the order of POD/ROM can be reduced further to tens by the balance truncation method [23].

2.3 Verification of the gust POD/ROM

A full-order unsteady CFD/CSD coupled aeroelastic solver should be used to generate the gust snapshots for constructing the gust POD/ROM. Our in-house multi-block structured CFD/CSD solver used in this research has been evaluated by many aeroelastic cases including two-dimensional airfoil model, wing model and full aircraft models [20–24]. To model a gust, the field velocity method proposed by Singh and Baeder was used in our in-house CFD/CSD solver, in which the arbitrary gust profile was introduced into the FVM-based CFD solver by utilizing grid velocity [35]. The field velocity method has been successfully realized and verified for simple and complex gust velocity profiles by many researchers such as Raveh [11, 12, 25], Bartels [14, 36] and Wang et al. [37].

The Goland+ wing model developed by Eastep and Olsen was used as a demonstrated case [38], which had been calculated by many researchers in transonic flutter prediction [24–27, 39, 40]. A 300-order gust POD/ROM of the Goland+ wing model in Mach number 0.82 was constructed according to the method described in Sections 2.1 and 2.2. Then ROM and the full-order CFD/CSD coupled solver are both used to calculate the gust responses due to the assigned gust profiles with the time step of 0.001 s. Here only the *z*-component of gust velocity is taken into account because usually the vertical gust is the most important in engineering. The 1-minus-cosine discrete gust profile is often used to evaluate the gust responses, which is defined as

$$\boldsymbol{w}_{\mathrm{g}}\left(t\right) = \frac{\boldsymbol{W}_{\mathrm{g}}}{\boldsymbol{V}_\infty}\left(1-\cos\frac{2\pi}{T_0}t\right), \quad t \leqslant T_0, \tag{16}$$

where $\boldsymbol{w}_{\mathrm{g}}$ and $\boldsymbol{W}_{\mathrm{g}}$ denote the gust relative velocity and gust velocity, T_0 is the period, and t is the time.

Figures 1 and 2 present the unsteady aerodynamic forces predicted by ROM and full-order CFD/CSD solver due to different periods of 1-minus-cosine discrete gust profiles (i.e. 10, 2, 1, 0.5 and 0.2 s) with the relative gust velocity of 0.01. Both Figures 1 and 2 show that the unsteady aerodynamic coefficients predicted by ROM agree well with those of the CFD/CSD solver. As shown in Figure 1, the gust responses are similar to the gust velocity profiles which disappear as soon as the gust finished. However, with the increase of the time period of the discrete gust profiles, the gust perturbation to the aerodynamic forces does not disappear but decreases gradually after the gust finished. Figure 2 shows that the shorter period or the higher frequency 1-minus-cosine gust generates more obvious and larger perturbation.

The leading five modes of the aeroelastic Goland+ wing model were taken into consideration in the gust simulation. The modal frequencies are 1.7051, 3.0516, 9.200, 10.906 and 13.493 Hz, respectively. Figure 3 shows the generalized modal displacement of the first two structural modes which presents the first bending and the first twist deformation. With the decrease of the periods or the increase of the frequencies of the gust profiles which are close to the structural modal frequencies, both the displacement perturbations of the two modes occur and become larger and larger after the gusts disappear. It is the unsteady structural deformation excited by the gust that generates the long time unsteady effects on the aerodynamic forces. It is different from a rigid model without such obviously long time unsteady nonlinear effects. Meanwhile, the displacement of mode 1 is much larger than that of mode 2 (i.e., near 10 times). It indicates that the low frequency bending modes are excited most easily by the gust. This result is very different from those obtained in flutter phenomena in which the unstable mode was usually dominant in twist [39–41]. The gust POD/ROM can catch these special phenomena of gust responses as well as the full-order CFD/CSD solver.

The results of the 1-minus-cosine gust indicate that the frequency of the gust has great impacts on the gust responses. In order to further verify the performance of the gust ROM, a complex gust profile plotted in Figure 4 is used, which is composed of multiple 1-minus-cosine and sine gust profiles with different frequencies and relative velocities. The comparison of gust responses of the lift and moment coefficients calculated by ROM and CFD/CSD solver is presented in Figure 5. The good agreement indicates that the constructed POD/ROM can catch the dominant nonlinear aerodynamic responses due to gust in transonic flow. It provides a good low-order state-space plant model for gust alleviation controller design.

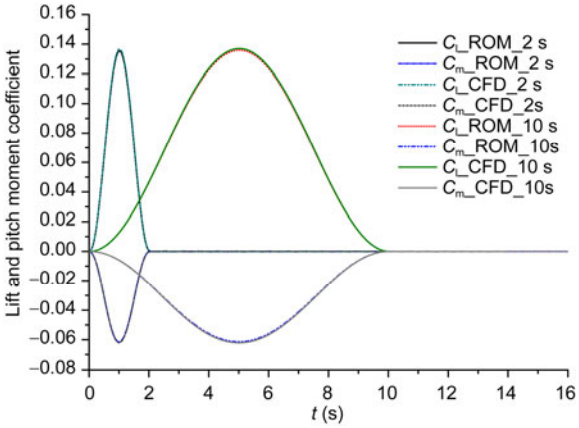

Figure 1 Unsteady aerodynamic coefficients due to gusts.

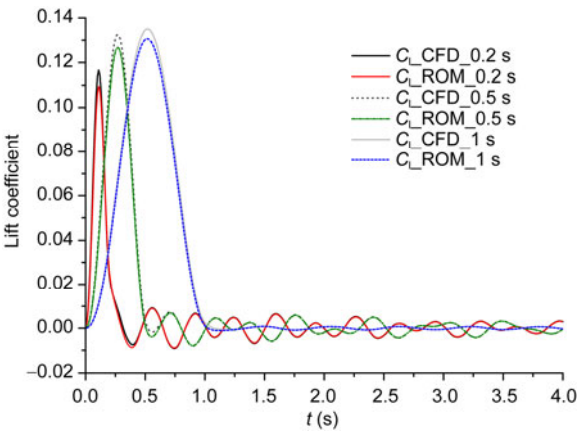

Figure 2 Unsteady lift coefficients due to different gusts.

3 Gust alleviation control law design

3.1 Aeroservoelastic ROM for active gust alleviation control

The open-loop aoeroelastic dynamic equation of a gust alleviation system with aerodynamic control surfaces is

$$\boldsymbol{M}v_{\mathrm{t}}+\boldsymbol{C}_{\mathrm{s}}v+\left(\boldsymbol{K}_0-\boldsymbol{K}_{\mathrm{f}}\right)u_{\mathrm{s}}=\boldsymbol{q}_\infty\boldsymbol{P}\boldsymbol{w}+\boldsymbol{q}_\infty\boldsymbol{D}_{\mathrm{g}}\boldsymbol{w}_{\mathrm{g}}+\boldsymbol{q}_\infty\boldsymbol{f}_{\mathrm{c}}, \quad (17)$$

where the $\boldsymbol{q}_\infty\boldsymbol{f}_{\mathrm{c}}$ is the unsteady aerodynamic forces due to the movement of the control surfaces. Adding the unsteady aerodynamic perturbation of the control flaps to the aeroelastic model in eq. (15), the augmented open-loop reduced order aeroservoelastic state equation is obtained as

$$\begin{bmatrix}\dot{\boldsymbol{w}}_{\mathrm{r}}\\ \dot{\boldsymbol{v}}_{\mathrm{m}}\\ \dot{\boldsymbol{u}}_{\mathrm{m}}\end{bmatrix}=\begin{bmatrix}-\boldsymbol{\Psi}_{\mathrm{r}}^{\mathrm{T}}A_0^{-1}\boldsymbol{H}\boldsymbol{\Psi}_{\mathrm{r}} & -\boldsymbol{\Psi}_{\mathrm{r}}^{\mathrm{T}}\boldsymbol{A}_0^{-1}\left(\boldsymbol{E}+\boldsymbol{C}\right)\boldsymbol{\Psi}_{\mathrm{m}} & -\boldsymbol{\Psi}_{\mathrm{r}}^{\mathrm{T}}\boldsymbol{A}_0^{-1}\boldsymbol{G}\boldsymbol{\Psi}_{\mathrm{m}}\\ \boldsymbol{q}_\infty\boldsymbol{M}_{\mathrm{m}}^{-1}\boldsymbol{\Psi}_{\mathrm{m}}^{\mathrm{T}}\boldsymbol{P}_{\mathrm{w}}\boldsymbol{\Psi}_{\mathrm{r}} & -\boldsymbol{M}_{\mathrm{m}}^{-1}\boldsymbol{C}_{\mathrm{m}} & -\boldsymbol{M}_{\mathrm{m}}^{-1}\boldsymbol{K}_{\mathrm{m}}\\ \boldsymbol{0} & \boldsymbol{I} & \boldsymbol{0}\end{bmatrix}$$

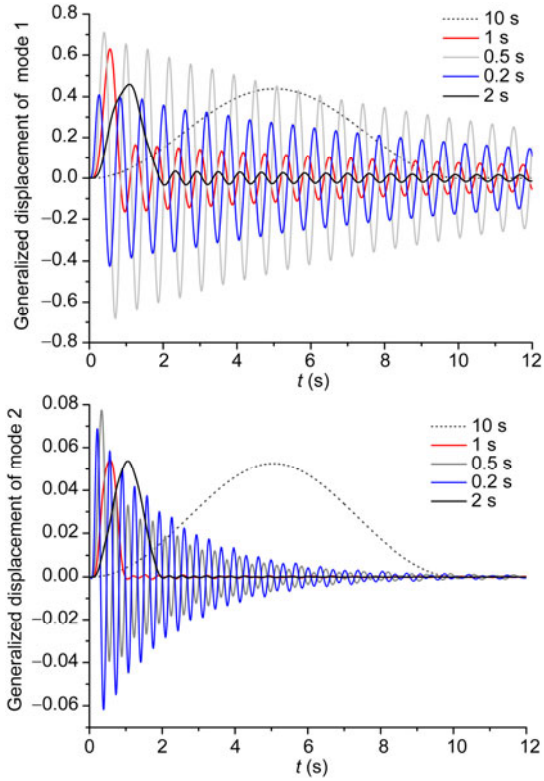

Figure 3 General modal displacements of the two leading modes.

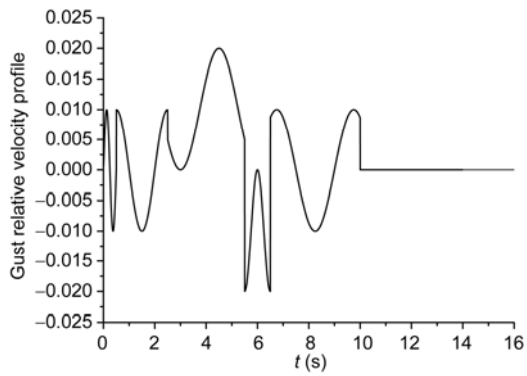

Figure 4 Gust profile time history.

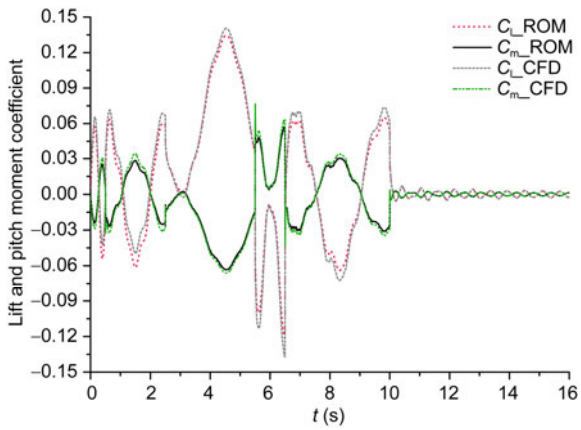

Figure 5 Comparison of unsteady aerodynamic forces.

$$\times\begin{bmatrix}\boldsymbol{w}_{\mathrm{r}}\\ \boldsymbol{v}_{\mathrm{m}}\\ \boldsymbol{u}_{\mathrm{m}}\end{bmatrix}+\begin{bmatrix}-\boldsymbol{\Psi}_{\mathrm{r}}^{\mathrm{T}}\tilde{\boldsymbol{D}}\\ \boldsymbol{q}_{\infty}\boldsymbol{\Psi}_{\mathrm{m}}^{\mathrm{T}}\boldsymbol{M}^{-1}\boldsymbol{P}_{\boldsymbol{w}_{\mathrm{g}}}\\ 0\end{bmatrix}\boldsymbol{w}_{\mathrm{g}}+\boldsymbol{q}_{\infty}\begin{bmatrix}-\boldsymbol{\Psi}_{\mathrm{r}}^{\mathrm{T}}\boldsymbol{P}_{\mathrm{w}\beta}\\ \boldsymbol{\Psi}_{\mathrm{m}}^{\mathrm{T}}\boldsymbol{M}^{-1}\boldsymbol{P}_{\mathrm{f}\beta}\\ 0\end{bmatrix}\beta, \tag{18}$$

where the β is the deflection of control surfaces, i.e., the leading-edge and rear-edge aerodynamic control surfaces of the wing; $\boldsymbol{P}_{\mathrm{w}\beta}$ is the aerodynamic perturbation matrix of the unit deflection of the control surfaces to the flow field variables, and $\boldsymbol{P}_{\mathrm{f}\beta}$ is the perturbation matrix of the unit deflection of the flap to the generalized aerodynamic forces. All of these unsteady aerodynamic influence matrices can be pre-computed by unsteady CFD/CSD solvers.

The structural inner force induced by the gust is necessary in gust load analysis. The relationship between structural loads and modal displacement is

$$\boldsymbol{f}=\boldsymbol{K}_{\mathrm{s}}\boldsymbol{u}_{\mathrm{s}}, \tag{19}$$

where $\boldsymbol{f}$ are load vectors such as bending moments, torsions and shear forces, $\boldsymbol{u}_{\mathrm{s}}$ are modal displacement vectors of the structural grid point, and $\boldsymbol{K}_{\mathrm{s}}$ is the stiffness matrix. In the generalized coordinates, the generalized structural stress loads is presented as

$$\boldsymbol{f}_{\mathrm{m}}=\boldsymbol{K}_{\mathrm{m}}\boldsymbol{\psi}_{\mathrm{m}}\boldsymbol{u}_{\mathrm{m}}, \tag{20}$$

where $\boldsymbol{K}_{\mathrm{m}},\boldsymbol{\psi}_{\mathrm{m}},\boldsymbol{u}_{\mathrm{m}}$ are the generalized modal stiffness, generalized modal vectors, and modal displacements respectively. The generalized structural gust stress load $\boldsymbol{f}_{\mathrm{m}}$ is expected to be suppressed by the gust alleviation system to improve the structural fatigue life, as well as the unsteady aerodynamic forces such as the lift and pitch moment coefficient affecting the ride quality. Thus, the open-loop aeroservoelastic model with gust alleviation system is rewritten as a general form:

$$\begin{cases}\dot{\boldsymbol{x}}=\boldsymbol{A}(\boldsymbol{q}_{\infty})\boldsymbol{x}+\boldsymbol{B}(\boldsymbol{q}_{\infty})\boldsymbol{\beta}+\boldsymbol{D}\boldsymbol{w}_{\mathrm{g}},\\ \boldsymbol{y}=\begin{bmatrix}0&0&0\\0&\boldsymbol{I}_{\mathrm{m}}&0\\0&0&\boldsymbol{I}_{\mathrm{m}}\end{bmatrix}\begin{bmatrix}\boldsymbol{w}_{\mathrm{r}}&\boldsymbol{v}_{\mathrm{m}}&\boldsymbol{u}_{\mathrm{m}}\end{bmatrix}^{\mathrm{T}}=\boldsymbol{C}\boldsymbol{x},\\ \boldsymbol{y}_{\mathrm{f}}=\begin{bmatrix}0&0&\boldsymbol{K}_{\mathrm{m}}\boldsymbol{\psi}_{\mathrm{m}}\end{bmatrix}\begin{bmatrix}\boldsymbol{w}_{\mathrm{r}}&\boldsymbol{v}_{\mathrm{m}}&\boldsymbol{u}_{\mathrm{m}}\end{bmatrix}^{\mathrm{T}}.\end{cases} \tag{21}$$

The inputs of the open-loop aeroservoelastic system are the deflection of the control surface $\boldsymbol{\beta}$. The output variable $\boldsymbol{y}$ is the structural response, i.e., the generalized displacement and velocity. The objective of the gust alleviation control law design problem is to find a feedback control law $\boldsymbol{\beta}=-\boldsymbol{K}\boldsymbol{f}(\boldsymbol{x},\boldsymbol{y})$ to improve the structural and aerodynamic gust responses.

3.2 Static output feedback control law design

In practical active aeroelastic control problems, the states related to nonlinear aerodynamics cannot be directly measured by sensors. Therefore the state-based controllers such as the classic LQR controller and many adaptive state feedback controllers require at least one state observer to estimate these state variables for feedback. However, the observers will reduce the robustness of the controller and meanwhile the real-time implementation of high-order controllers is also quite problematic. Rather than state feedback controllers (i.e., LQR and LQG controllers), the optimal static output feedback (SOF) controller is only based on the direct feedback of the sensors' output, which is very suitable for the active control law design based on the aeroelastic ROM [41].

An optimal SOF controller aims to find constant feedback gains to optimize the given performance index. A very brief introduction of SOF control is presented here and the details can be found in many publications [42, 43]. For an nth-order LTI system:

$$\begin{cases}\dot{\boldsymbol{x}}=\boldsymbol{A}\boldsymbol{x}+\boldsymbol{B}\boldsymbol{u}+\boldsymbol{D}\boldsymbol{w},\\ \boldsymbol{y}=\boldsymbol{C}\boldsymbol{x},\end{cases} \tag{22}$$

where $\boldsymbol{x}$ is the system state variable, $\boldsymbol{A}$ is the system dynamic matrix in state-space form, $\boldsymbol{u}$ is the command of the actuator, $\boldsymbol{B}$ is the control matrix, $\boldsymbol{y}$ is the measurement of the sensors, $\boldsymbol{C}$ is the matrix relating the sensor's measurements to the state variables, $\boldsymbol{w}$ is the zero-mean unit intensity white noise process, and $\boldsymbol{D}$ is the matrix of noise intensity. Suppose the constant gain output feedback control law as the form:

$$\boldsymbol{u}(t)=-\boldsymbol{K}\boldsymbol{y}(t), \tag{23}$$

the feedback gain $\boldsymbol{K}$ can be determined by minimizing the quadratic performance:

$$\boldsymbol{J}=\frac{1}{2}\int_0^{\infty}\left[\boldsymbol{x}^{\mathrm{T}}(t)\boldsymbol{Q}\boldsymbol{x}(t)+\boldsymbol{u}^{\mathrm{T}}(t)\boldsymbol{R}\boldsymbol{u}(t)\right]\mathrm{d}t, \tag{24}$$

where $\boldsymbol{Q}$ and $\boldsymbol{R}$ are the pre-selected positive matrices. The solution to the above optimization problem is [41, 42]:

$$\begin{cases}\boldsymbol{K}=\boldsymbol{R}^{-1}\boldsymbol{B}^{\mathrm{T}}\boldsymbol{S}\boldsymbol{P}\boldsymbol{C}^{\mathrm{T}}(\boldsymbol{S}\boldsymbol{P}\boldsymbol{C})^{-1},\\ (\boldsymbol{A}+\boldsymbol{B}\boldsymbol{K}\boldsymbol{C})^{\mathrm{T}}\boldsymbol{S}+\boldsymbol{S}(\boldsymbol{A}+\boldsymbol{B}\boldsymbol{K}\boldsymbol{C})-\boldsymbol{C}^{\mathrm{T}}\boldsymbol{K}^{\mathrm{T}}\boldsymbol{R}\boldsymbol{K}\boldsymbol{C}+\boldsymbol{Q}=0,\\ (\boldsymbol{A}+\boldsymbol{B}\boldsymbol{K}\boldsymbol{C})\boldsymbol{P}+\boldsymbol{P}(\boldsymbol{A}+\boldsymbol{B}\boldsymbol{K}\boldsymbol{C})^{\mathrm{T}}+\boldsymbol{D}\boldsymbol{D}^{\mathrm{T}}=0.\end{cases} \tag{25}$$

The unknown matrices $\boldsymbol{P}$, $\boldsymbol{S}$ and $\boldsymbol{K}$ can be calculated by many iterative algorithms, i.e., Newton-Raphson's method and BFGS method [42, 43].

4 Simulation and results

4.1 MIMO gust alleviation control scheme

The gust alleviation controller aims to improve the ride

quality related to the gust unsteady aerodynamic forces, reduce the structural gust loads due to the structural deformation, and improve the structural fatigue life due to the structural vibration velocity. The objectives of the MIMO SOF gust alleviation controller include: (i) reducing the gust aerodynamic coefficient by not less than 50% to improve ride quality, because the gust perturbation to unsteady aerodynamic coefficients has great impact on the rigid dynamics; (ii) reducing the maximum structural stress due to gust by not less than 20%; (iii) reducing the generalized modal velocity of mode 1 by not less than 30% during the gust and stabilizing the generalized modal velocity as soon as possible, which would obviously improve the structural fatigue safety. The Goland+ wing model with the span of 6.096 m and the chord length of 1.8288 m is modified slightly by adding four control surfaces at the leading-edge (LE) and trailing-edge (RE) to demonstrate the MIMO active gust alleviation control scheme. As presented in Figure 6, these control surfaces (i.e., REO, REI, LEO, and LEI) are the same size of length 1.12 m and width 0.43 m.

In Section 2.3 it has been founded that the first low frequency bending mode is excited most easily by the gust and the others are much smaller. So it is better to select the first bending modes as the dominant feedback signal. Considering that the structural twist mode may have great impact on the local angle of the attack, the structural velocity of the second structural mode is also selected as the feedback signal. Thus, a lower-order SOF controller (4×3) is defined as

$$\boldsymbol{\beta} = \begin{bmatrix} K_{11} & \cdots & K_{14} \\ \vdots & \vdots & \vdots \\ K_{41} & \cdots & K_{44} \end{bmatrix} \begin{bmatrix} \xi_1 \\ \xi_2 \\ \dot{\xi}_1 \\ \dot{\xi}_2 \end{bmatrix}. \tag{26}$$

The open-loop aerosevoelastic state-space model was constructed based on the evaluated 300-order POD/ROM in Section 2.3. For the convenience to control design, it then was reduced further to a 50-order POD/BT-ROM model by balanced truncation method [25]. The designed constant control gain [0.001, 0.205, 0.0053, –0.022; 0.0011, 0.20, 0.005, –0.02; 0.102, 0.002, 0.031, 0.064; 0.10, 0.0013, 0.03, 0.06]^{T} is determined according to the above-mentioned SOF algorithm.

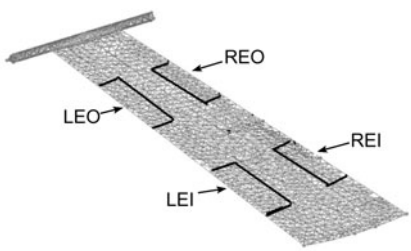

Figure 6 Modified Goland+ wing with four control surfaces.

4.2 Gust alleviation for discrete 1-minus-cosine gust

The discrete 1-minus-cosine gust is often used to evaluate the gust alleviation performance. Figures 7–9 present the transonic gust responses of the Goland+ wing model in Mach 0.82 with and without the controller. The period of the gust is 2 s. The curves of the gust responses of the closed-loop predicted by the full-order CFD/CSD solver and the ROM agree well, which indicates that ROM has good accuracy and is capable of catching the dominant nonlinear behaviors of the aeroelastic model in transonic flow. The unsteady lift and pitch moment coefficients during the gust are reduced by 54% and 71%. The generalized velocity of mode1 is reduced by 67%. Figure 8 shows that there is an obvious large gust excited vibration of the generalized velocity. The frequency is very close to the natural frequency of the first bending mode. However, the gust alleviation controller can suppress the vibration very quickly. In Figure 9, it can be seen that the maximum of the generalized structural inner stress is reduced by 21%. The vibration of structural stress exited by the gust is also suppressed quickly once the gust disappears. The deflections of the control surfaces presented in Figure 10 are not more than 0.03, which is easy to be realized and also only produce very small perturbation to the rigid body movement. The agreement of the commands predicted by ROM and the CFD/CSD solver verifies the capability of ROM in gust alleviation.

Figures 11–13 present the gust responses calculated by ROM due to the 1-minus-cosine gust with the period of 0.2 s. For the open-loop aeroelastic system, all the gust responses were excited by the high frequency gust. It is obvious that the vibrations of these responses exist for a long time after the gust disappears, such as the aerodynamic response in Figure 11, the generalized velocity response in Figure 12, and the generalized maximum structural stress in Figure 13. Although finally the gust responses will gradually disappear in nearly 40 s after the gust finishes, the excited such large structural velocity and stress will do harm to the structural fatigue life and reduce the lift of the aircraft. With the gust alleviation controller, the peak values of the lift and pitch moment during the gust are reduced by 57% and 62% respectively. The peak values of the generalized structural velocity and stress during the gust are also reduced by 64% and 22%, respectively. The control performance of the controller is capable of keeping nearly the same for different frequency gust. The excited gust responses can be suppressed as quickly as in 4 s with the controller. Meanwhile, as shown in Figure 14, the maximum control commands are still very small and no more than 0.06.

4.3 Gust alleviation for a sequence of 1-minus-cosine and sin gust

In this section a multiple discrete 1-minus-cosine and sin gust presented in Figure 15 is used to further evaluate the

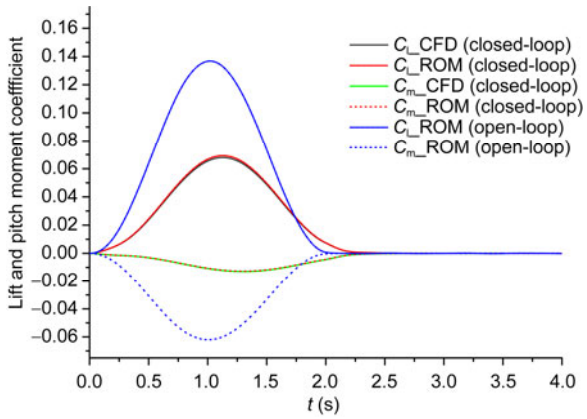

Figure 7 Unsteady aerodynamics of open-loop and closed-loop.

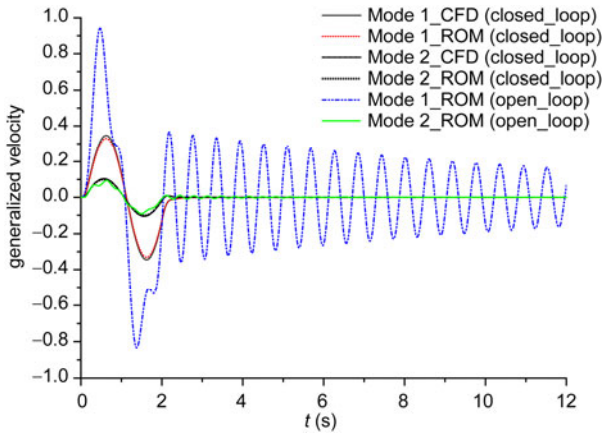

Figure 8 Generalized velocity of open-loop and closed-loop.

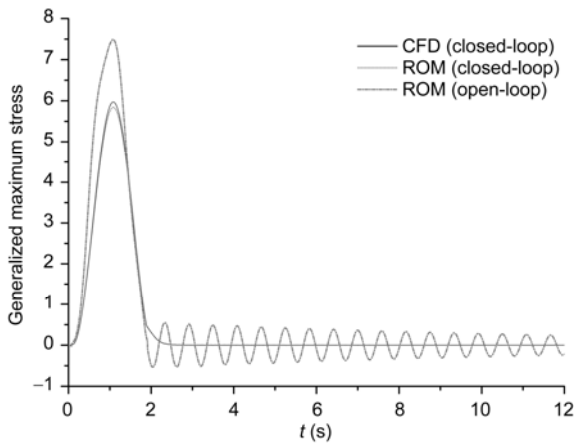

Figure 9 Generalized maximum stress of open-loop and closed-loop.

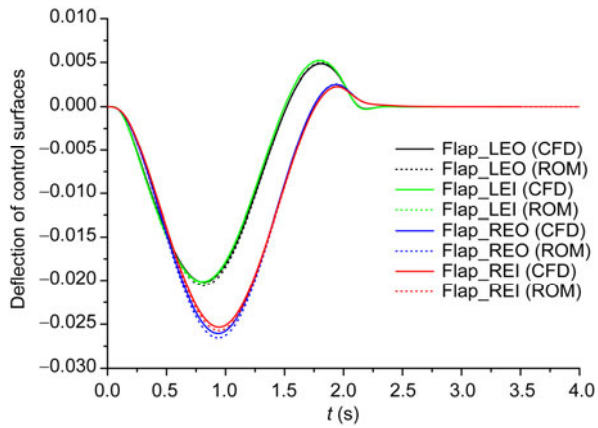

Figure 10 Comparison of the control commands.

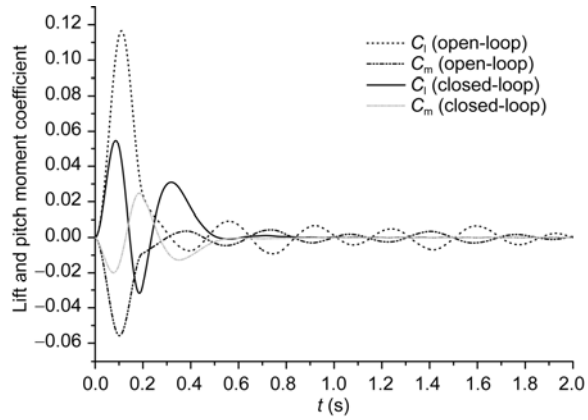

Figure 11 Unsteady aerodynamics of open-loop and closed-loop.

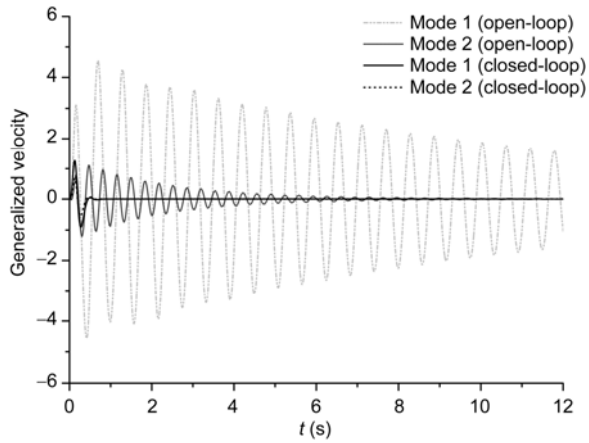

Figure 12 Generalized velocity of open-loop and closed-loop.

control performance of the designed SOF control law. It can be seen in Figure 16 that the gust unsteady aerodynamic responses can be well alleviated. Both the lift and pith moment coefficients due to the gust are reduced by more than 50%. Figure 17 presents the generalized structural velocity excited by the gust. It can be found again that the first bending mode is excited the most by the gust and the second twist mode is excited much little. The excited structural velocities are suppressed by the gust alleviation controller greatly, especially for the first bending mode which is reduced by more than 70%. Figure 18 presents the structural maximum inner stress response excited by the gust. In the open-loop aeroelastic system, the large and high frequency vibration of the stress excited by the gust is very

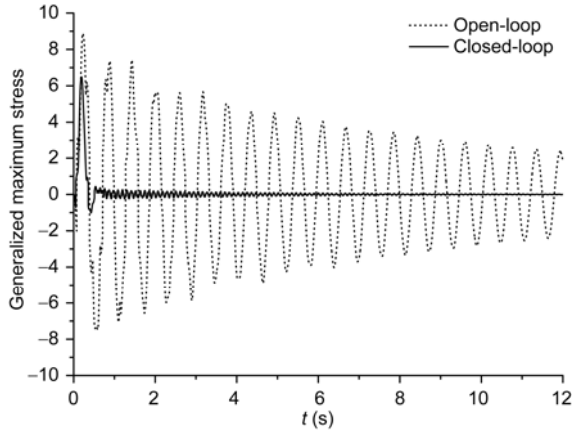

Figure 13 Generalized maximum stress of open-loop and closed-loop.

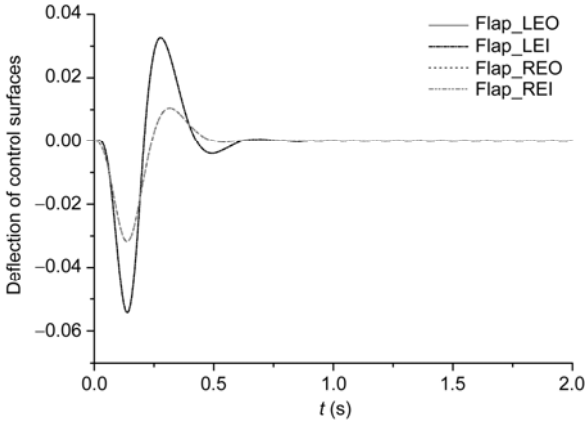

Figure 14 Comparison of the control commands.

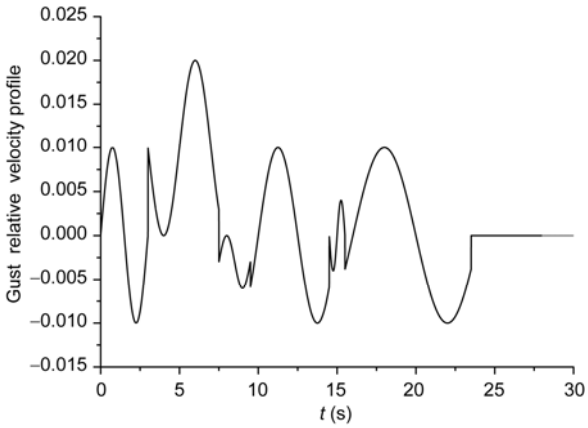

Figure 15 Gust relative velocity time history.

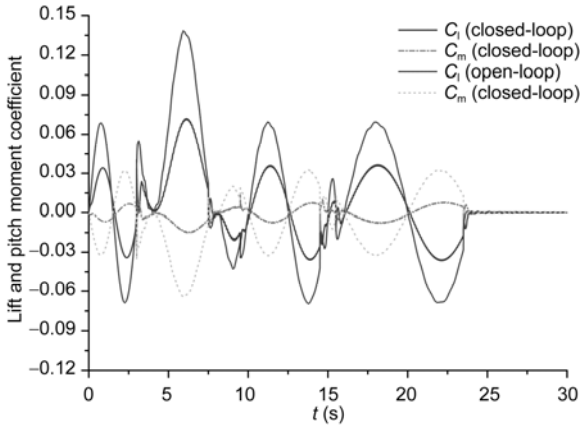

Figure 16 Gust responses of aerodynamic forces.

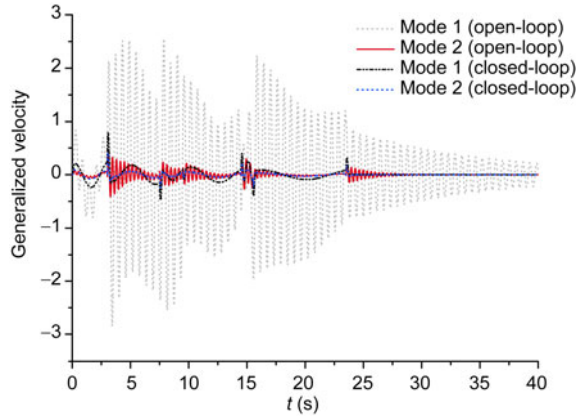

Figure 17 Gust responses of structural velocity.

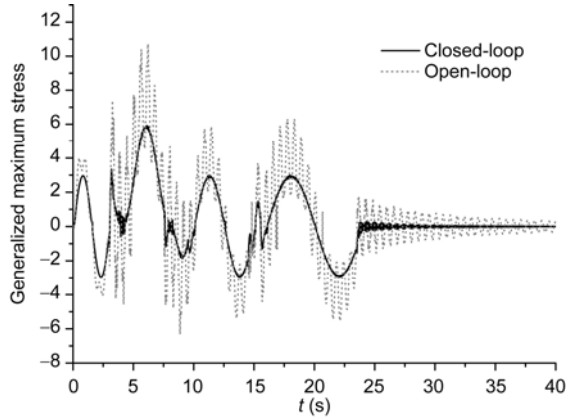

Figure 18 Gust responses of structural inner stress.

harmful to the health of the wing structure. However the controller can successfully suppress them with the reduction of more than 30%. Figure 19 presents the deflection of the control surfaces. The peak value of the control commands is no more than 0.035 and the variation of the command is not so large, which is convenient to be realized by hardware.

The simulation results indicate that the designed simple SOF controller can alleviate the gust responses in transonic flow with good performance in different gust profiles. The gust POD-ROM is capable of catching the dominant transonic aeroelastic behaviors in gust, which provide a useful reduced order model for gust analysis and gust alleviation for elastic aircrafts.

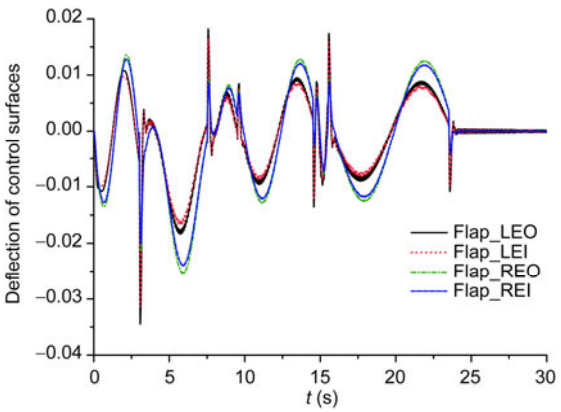

Figure 19 Control commands of the control surfaces.

5 Conclusions

Gust alleviation is one of the key technologies in modern high-speed elastic aircraft design. In transonic flow regime, the traditional gust analysis method based on linear aerodynamic panel model is not accurate enough for gust alleviation controller design. A POD-based reduced order modeling of gust responses in transonic flow was proposed and verified. The simulation results indicate that the proposed gust POD/ROM can catch the dominant nonlinear gust responses in transonic flow with good accuracy. POD/ROM provides a good low-order state space model for gust alleviation controller design. An output feedback MIMO gust alleviation control law was designed and demonstrated by the Goland+ wing aeroelastic model. The simulation results of different discrete gust cases show the good performance of the controller. In the future, the proposed method can be integrated with the flight controller of a fully flexible aircraft. It can be also extended to morphing aircrafts and very large flexible aircraft such as Helios. The simulation is carried out in the ideal theory condition without taking into account the time-delay and nonlinear mechanism of the hardware, which can also be further investigated in the detail design of the active controller.

The work was partially supported by the National Natural Science Foundation of China (Grant Nos.11272005, 10902082, 91016008).

1 Code of Federal Regulations, Aeronautics and Space, Part 25.341. Gust and turbulence loads. Maryland: Office of Federal Register, National Archives and Records Administration, January 2003
2 Robert C, Michael J A, Ryan P D, et al. Fight test of the f/a-18 active aeroelastic wing airplane. NASA/TM-2005-213664, 2005
3 Simpson J, Suleman A, Cooper J. Review of European research project active aeroelastic aircraft structures. In: IFASD Conference, Munich, 2005
4 Gur O, Bhatia M, Schetz J, et al. Design optimization of a truss-braced-wing transonic transport aircraft. J Aircraft, 2010, 47(6): 1907–1917
5 Moulin B, Karpel M. Gust loads alleviation using special control surfaces. J Aircraft, 2007, 44(1): 17–24
6 Vartio E J, Shaw E E, Vetter T. Gust load alleviation flight control system design for a sensorcraft vehicle. AIAA 2008-7192, 2008
7 Shao K, Wu Z, Yang C, et al. Design of an adaptive gust response alleviation control system: simulations and experiments. J Aircraft, 2010, 47(3): 1022–1029
8 Ricci S, Scotti A. Gust response alleviation on flexible aircraft using multi-surface control. AIAA 2010-3117, 2010
9 Zeng J, Moulin B, Callafon R. Adaptive feed-forward control for gust load alleviation. J Guid Control Dynam, 2010, 33(3): 862–872
10 Christopher D R, Christine V J. Survey of applications of active control technology for gust alleviation and new challenges for lighter-weight aircraft. NASA/TM-2012-216008, 2012
11 Raveh D E. CFD-based models of aerodynamic gust response. J Aircraft, 2007, 44(3): 888–897
12 Raveh D E. Gust-response analysis of free elastic aircraft in the transonic flight regime. J Aircraft, 2011, 48(4): 1204–1211
13 Robert G C, Rafael P, Paul G. Robust gust alleviation and stabilization of very flexible aircraft. AIAA J, 2013, 51(2): 330–340
14 Robert E B. Development, verification and use of gust modeling in the NASA computational fluid dynamics code fun3d. NASA/TM–2012-217771, 2012
15 Silva W A. Identification of nonlinear aeroelastic systems based on the volterra theory: progress and opportunities. Nonl Dyn, 2005, 39: 25–62
16 Chen G, Zuo Y, Sun, J, et al.Support-vector-machine-based reduced-order model for limit cycle oscillation prediction of nonlinear aeroelastic system. Math Probl Eng, doi:10.1155/2012/152123, 2012
17 Lieu T, Farhat C. Adaptation of aeroelastic reduced-order models and application to an f-16 configuration. AIAA J, 2007, 45 (6): 244–1257
18 Beran P S, Lucia D J. A reduced order cyclic method for computation of Limit Cycles. Nonl Dyn, 2005, 39: 143–158
19 Gaetan K, Jean-claude G, Alexander F W, et al. The method of proper orthogonal decomposition for dynamical characterization and order reduction of mechanical systems: an overview. Nonl Dyn, 2005, 41: 147–169
20 Custer C H, Thomas J P, Dowell E H, et al. A nonlinear harmonic balance method for the cfd code OVERFLOW 2. International Forum on Aeroelasticity and Structural Dynamics, 2009-050, Seattle, 2009
21 Badcock K J, Woodgate M A. Bifurcation prediction of large-order aeroelastic models. AIAA J, 2010, 48(6): 1037–1046
22 Chen G, Li Y M, Yan G R. A nonlinear pod reduced order model for limit cycle oscillation prediction. Sci China Phys Mech Astron, 2010, 53(6): 1325–1332
23 Chen G, Li Y M, Yan G R. Active control stability/augmentation system design based on reduced order model. Chin J Aeronaut, 2010, 23(6): 637–644
24 Chen G, Li Y M, Yan G R. Limit cycle oscillation prediction and control design method for aeroelastic system based on new nonlinear reduced order model. Int J Comput Meth, 2011, 8(1): 77–90
25 Chen G, Sun J, Li Y M. Active flutter suppression control law design method based on balanced proper orthogonal decomposition reduced order model. Nonl Dyn, 2012, 70: 1–12
26 Chen G, Sun J, Li Y M. Adaptive reduced-order-model-based control law design for active flutter suppression. J Aircraft, 2012, 49(4): 973–980
27 Zaide A, Raveh D E. Numerical simulation and reduced-order modeling of airfoil gust response. AIAA J, 2006, 44(8): 1826–1834
28 Sohrab H, Hugh H T L, Joaquim R R A. A model-predictive gust load alleviation controller for a highly flexible aircraft. J Guid Control Dynam, 2012, 36(6): 1751–1766
29 Ronch A D, Badcock K J, Wang Y, et al. Nonlinear model reduction for flexible aircraft control design. AIAA -2012-4404, 2012
30 Mukhopadhyay V. Historical perspective on analysis and control of aeroelastic responses. J Guid Control Dynam, 2003, 26(5): 673–684

31 Kumar V S, Laura A M, Raymond K, et al. Receptance based active aeroelastic control using multiple control surfaces. AIAA- 2012-1485, 2012
32 Karpel M, Moulin B, Presente E, et al. Dynamic gust loads analysis for transport aircraft with nonlinear control effects. AIAA-2008-1994, 2008
33 Lesoinne M, Sarkis M, Hetmaniuk U, et al. A linearized method for the frequency analysis of three-dimensional fluid/structure interaction problems in all flow regime. Comput Meh Appl Mech Eng, 2001, 190: 3121–3146
34 Holmes P, Lumley J L, Berkooz G. Turbulence, Coherent Structures, Dynamical Systems and Symmetry. Cambridge: Cambridge University Press, 1996
35 Singh R, Baeder J D. Direct calculation of three-dimensional indicial lift response using computational fluid dynamics. J Aircraft, 1997, 34(4): 465–471
36 Bartels R E. Uncertainty due to fluid/structure interaction for the aeroelastic vehicle traversing the transonic regime. AIAA-2012-1631, 2012
37 Wang Z, Zhang Z, Chen P C, et al. A compact cfd-based reduced order modeling for gust analysis. AIAA-2011-2041, 2011
38 Eastep F E, Olsen J J. Transonic flutter analysis of a rectangular wing with conventional airfoil sections. AIAA J, 1980, 18(10): 1159–1164
39 Beran P S, Strganac T W, Kim K, et al. Studies of store-induced limit-cycle oscillations using a model with full system nonlinearities. Nonlinear Dynam , 2004, 37: 329–339
40 Ali H N, MehdiG., Hajj LR. Normal form representation of the aeroelastic response of the Goland wing. Nonl Dyn, 2012, 67: 1847–1861
41 Mayuresh J P, Dewey H H. Output feedback control of the nonlinear aeroelastic response of a slender wing. J Guid Control Dynam, 1992, 25(2) :302–308
42 Syrmos V L, Abdallah C T, Dorato P, et al. Static output feedback: A survey. Automatica, 1997, 33(2):125–137
43 Jacob E, Arie W. A result on output feedback linear quadratic control. Automatica.2008, 44: 265–271